energies

MDPI

Article

Investigating Response to Voltage, Frequency, and Phase Disturbances of Modern Residential Loads for Enhanced Power System Stability

Obaidur Rahman [1], Sean Elphick [1], Duane A. Robinson [1,*] and Jenny Riesz [2]

[1] Australian Power Quality Research Centre, University of Wollongong, Wollongong 2522, Australia; orahman@uow.edu.au (O.R.); elpho@uow.edu.au (S.E.)
[2] Australian Energy Market Operator, Brisbane 4000, Australia; jenny.riesz@aemo.com.au
* Correspondence: duane@uow.edu.au

Abstract

This paper presents experimental testing results which describe the response of modern residential loads and electric vehicle (EV) chargers to various voltage magnitude, frequency, and phase angle disturbances. The purpose of these tests is to replicate real life network conditions and assist Network Service Providers and the Australian Energy Market Operator in identifying and predicting potential power variation and system stability issues caused by load behaviour during power system transient phenomena. By examining the behaviour of typical loads connected to distribution networks, a deeper understanding of their response can be achieved, enabling the refinement of composite load models that are compatible with the Western Electricity Coordinating Council dynamic composite load model (CMPLDW) structure presently used for dynamic studies. The performance of a wide range of common appliances found in residential settings, such as refrigerators, microwave ovens, air conditioners, direct-on-line motor-based appliances, and EV chargers, has been evaluated. The results obtained from these tests offer valuable insights into the behaviour of different load types and illustrate differing performances from established model parameters, identifying the need to refine existing CMPLDW models. The results also support the reclassification of several appliances within the composite load model, motivate the introduction of a dedicated EV charger component, and empower network operators to improve the modelling of modern power network responses.

Keywords: composite load models; power system faults; voltage sags; stability

Check for updates

Academic Editor: Tao Lin

Received: 2 December 2025
Revised: 14 January 2026
Accepted: 16 January 2026
Published: 19 January 2026

Copyright: © 2026 by the authors. Licensee MDPI, Basel, Switzerland. This article is an open access article distributed under the terms and conditions of the Creative Commons Attribution (CC BY) license.

1. Introduction

Precise load modelling is essential for Network Service Providers (NSPs) to evaluate power system performance under various operating conditions, assess network stability issues, and devise effective control solutions [1,2]. In recent years, power systems worldwide have undergone major transformation with the introduction of distributed energy resources (DERs) and modern flexible loads. In the Australian National Electricity Market (NEM), this transformation is especially pronounced at low voltage, where inverter interfaced photovoltaic (PV) systems, battery energy storage systems (BESSs), electric vehicle (EV) chargers, and electronically controlled appliances now contribute a significant share of residential demand [3–6]. When subjected to faults and other disturbances, power systems that incorporate these devices exhibit dynamic behaviours [4,5] which traditional static load models used by NSPs are incapable of capturing. The present load models used

by the Australian Energy Market Operator (AEMO), Brisbane, Australia, known as ZIP (impedance-, current-, and power-based) models, were last calibrated and validated in 1999, and they are unable to accurately model the complex dynamic behaviour of modern loads [7]. Accurately representing these behaviours is therefore critical for studies of voltage stability, frequency stability, and post-fault recovery in systems with high penetrations of DERs and electronically interfaced loads [3,8–10].

Sophisticated composite load models are now available that can capture both the dynamic and static response of loads [8]. Composite load models consider the diverse aspects of load behaviour, such as dynamic response, sensitivity to voltage changes, and response to frequency fluctuations. In order to better model the response of modern power systems, the Western Electricity Coordinating Council (WECC), Salt Lake City, UT, USA, has developed an advanced composite load model (termed CMPLDW) with various components, including different types of motor loads and electronic/static loads, as well as the inclusion of DERs [11]. The addition of electrical distance between the transmission network and end load also allows this model to capture delayed voltage recovery events from transmission faults [12,13]. The North American Electricity Reliability Corporation (NERC), Washington, DC, USA, recommends the use of the CMPLDW model for dynamic studies in power systems [14]. However, the model incorporates complex load characteristics, which requires the input of as many as 133 parameters. The model is constantly updated using inputs from NSPs, through the utilisation of data measured during power system faults and laboratory testing of appliances. Recent studies and reviews have highlighted that, despite progress, parameterisation of composite load models remains heavily influenced by legacy motor-driven equipment and large commercial and industrial installations, with relatively limited empirical data for modern residential appliances and EV charging infrastructure [3,8,15].

In the context of the NEM, several factors motivate a more detailed characterisation of residential loads. First, the composition of household demand is changing, with traditional direct-on-line motor loads being progressively replaced by inverter-based air conditioners, LED lighting, switch mode power supplies, and controllable EV chargers. Second, distribution-level measurements suitable for model identification are sparse and often affected by network events and unobserved customer behaviour. Third, existing composite load models do not explicitly represent emerging technologies such as residential EV chargers, for which the disturbance response depends on both the charger and vehicle control strategies [9,16]. These issues introduce significant uncertainty into dynamic load representations for planning and operational studies in distribution networks containing high penetration of DER.

Existing load modelling approaches range from static representations such as ZIP models to dynamic motor and composite RMS models used in disturbance and voltage recovery studies. While these models remain practical for many applications, modern residential demand includes a growing share of electronically interfaced loads and controllable charging that can exhibit protection-driven behaviour under disturbances. These characteristics can be under-represented when modern appliances and EV charging are grouped into legacy static or motor-dominated components without measurement-based tuning. This motivates the experimental focus of this paper and the modelling implications derived from the measured responses.

The work presented in this paper was undertaken in collaboration with the Australian Energy Market Operator (AEMO) as part of a CSIRO-funded research program investigating distributed energy resources and stability [17,18]. Specifically, the work involved extensive experimental evaluation of the performance of modern loads when subject to various voltage magnitude, frequency, and phase angle disturbances which were

designed to replicate real life network disturbances. The experimental work focused on a representative set of residential appliances, including refrigerators, microwave ovens, air conditioners, heaters, fans, LED lighting, motor-based equipment, and both Level 1 and Level 2 EV chargers. Each device was subjected to systematic sets of voltage sag and swell, frequency, and phase angle jump disturbances to quantify the active and reactive power response. The objective was to obtain information on the response of typical loads connected to distribution networks, enabling a better comprehension of their behaviour, and facilitating updates to the parameters of the CMPLDW load models. More specifically, the contributions of this paper are as follows:

(i) It provides a comprehensive set of laboratory measurements of the electrical performance of modern residential loads and EV chargers under realistic grid disturbance scenarios that are relevant for the NEM.
(ii) It identifies behaviours that are not captured by the present Root Mean Squared (RMS) composite load model, including capacitor current overshoots, stalled motor operation, and voltage-dependent disconnection and reconnection of electronic loads.
(iii) It proposes revised classifications and parameterisation guidelines for the CMPLDW load components and highlights the need for a dedicated EV charger block for future composite load model implementations. These results are intended to support AEMO and NSPs in improving the accuracy of dynamic load modelling in stability studies for emerging, high-DER power systems [11–16].

This paper is focused on the experimental measurement of residential load behaviour under disturbances that are commonly studied using composite load models. The purpose is to use the measured responses to support improved load classification and tuning of parameter values used in existing composite load modelling practice, including parameter sets used by EPRI and other utilities. The work does not propose a new composite load model structure.

The remainder of the paper is organised as follows:

- Section 2 summarises the WECC CMPLDW model;
- Section 3 describes the disturbance test design and laboratory setup;
- Sections 4 and 5 present the experimental results for household loads and EV chargers, respectively;
- Section 6 discusses key findings and modelling recommendations;
- Section 7 concludes the paper and outlines directions for future work.

2. WECC Composite Load Model

This section summarises the basic components of the CMPLDW load model, including its overall structure, types of loads, and input parameters. The structure of the CMPLDW model is depicted in Figure 1 and consists of the following key components:

1. A distribution transformer with an on-load tap changer, where the transformer impedance is represented as jXxf.
2. A substation shunt capacitor, where Bss is the susceptance.
3. A single-phase equivalent model of the distribution feeders that carry power to the end-use loads (Rfdr + jXfdr). Shunt capacitors are implemented at both ends to account for reactive power losses in the feeder, ensuring that the net apparent power at the transmission bus matches that of the power flow case.
4. Six different classifications of loads which are connected to the load bus, including a combination of four different types of motors, an equivalent electronic load model, and the remaining loads combined into a static polynomial load model.

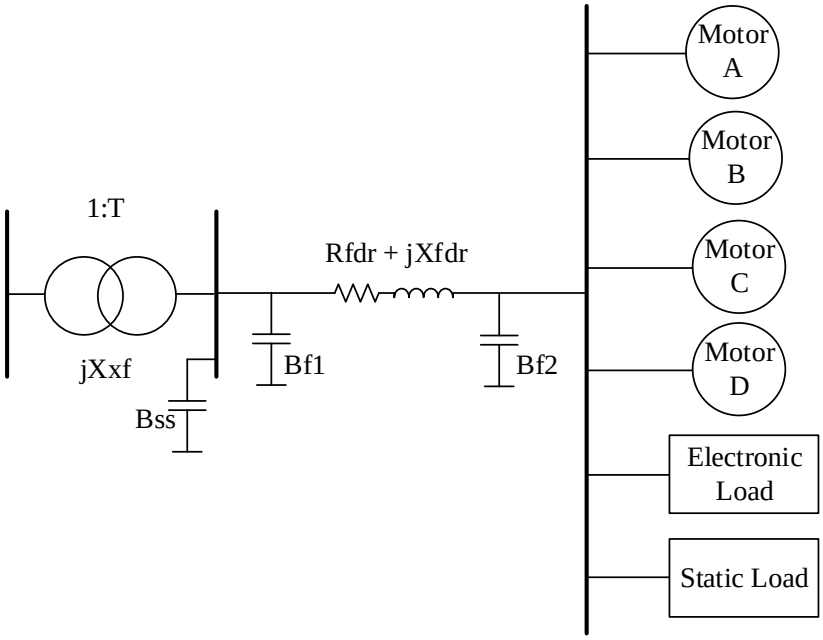


Figure 1. WECC composite load model structure.

The six different classifications of load types in the CMPLDW model are summarised in Table 1.

Table 1. Classification of the different types of loads in CMPLDW.

Motor A	Refers to 3-phase induction motors that have high locked-rotor torque and low inertia (with an H value of 0.1 s) and are designed to drive constant torque loads. These types of motors are typically used in commercial and industrial air conditioning compressors and refrigeration systems.
Motor B	Another 3-phase induction motor, but with high inertia (with an H value ranging from 0.25 s to 1.0 s), which is designed to drive loads whose torque is proportional to the speed squared. These motors are commonly used in commercial ventilation fans and air-handling systems, with typical ratings of 4 kW to 19 kW.
Motor C	A 3-phase induction motor that has low inertia (with an H value ranging from 0.1 s to 0.2 s) and is designed to drive loads whose torque is proportional to the speed squared. These motors are typically used in commercial water circulation pumps in central cooling systems, with typical ratings of 4 kW to 19 kW.
Motor D	A specialised performance model that is specifically designed to represent single-phase (1P) compressors. These motors have a constant torque load characteristic and minimal inertia, which can make them prone to stalling. They are commonly used in single-phase residential and light commercial refrigerator compressor motors in Australia, with typical ratings of 2 kW to 4 kW.
Power Electronic	A power electronic load refers to electronic devices used by consumers (such as computers and televisions), appliances (e.g., dishwashers), office equipment, and variable frequency drives (VFDs) used in commercial and industrial settings.
Static	A static load represents the remaining unclassified aggregate loads, including constant impedance loads such as incandescent lighting.

3. Load Testing Methodology

3.1. List of Disturbances

The different types of disturbances applied to the loads were split up into frequency, voltage magnitude (sags and swells), and phase angle jumps. Details for each disturbance type are summarised below.

3.1.1. Voltage Magnitude Disturbances

For voltage magnitude disturbances, both voltage sags and swells of varying durations and magnitudes were considered. Tables 2 and 3 summarise the list of voltage sag and swell tests which have been applied to the loads, with the magnitude of the retained voltage expressed in per unit (pu) and duration of the sag or swell at the retained voltage expressed in milliseconds (ms). A total of 21 voltage sag tests and 18 voltage swell tests were applied to each of the individual loads.

Table 2. Voltage sag magnitude and duration.

Voltage Sag Magnitude (pu)	Duration of Sag (ms)		
0.8	80	120	220
0.7	80	120	220
0.6	80	120	220
0.5	80	120	220
0.4	80	120	220
0.3	80	120	220
0.2	80	120	220

Table 3. Voltage swell magnitude and duration.

Voltage Swell Magnitude (pu)	Duration of Swell (ms)		
1.05	80	120	220
1.1	80	120	220
1.125	80	120	220
1.15	80	120	220
1.175	80	120	220
1.2	80	120	220

3.1.2. Frequency

Table 4 summarises the frequency disturbances that were applied to the loads under test. This includes a frequency step change of +2 Hz and −3 Hz. These values were selected by analysing the available frequency data from AEMO, which indicated the maximum excursion for frequency being limited to between 47 and 52 Hz. The loads were also tested to evaluate how they responded to ramped frequency variations, i.e., the rate of change of frequency (RoCoF) characteristics. The rates of change of frequencies were selected to be 0.4, 1, and 4 Hz/s. For the RoCoF tests, the lower and upper thresholds of the frequency were again 47 and 52 Hz, respectively.

Table 4. List of frequency disturbances.

Frequency Disturbance Type	Frequency Change (ΔF)
Step Frequency	−3 Hz
	+2 Hz
Ramp Frequency Variations (RoCoF)	±0.4 Hz/s
	±1 Hz/s
	±4 Hz/s

3.1.3. Phase Angle Jump

Table 5 summarises the list of phase angle jumps that were applied to ascertain the load response.

Table 5. List of phase angle jumps.

Disturbance Type	Phase Angle Change (Δθ)
Phase jump due to asymmetric fault	±15° ±30° ±45° ±60° ±90°

3.2. Load Types

Table 6 list the loads selected for testing. These loads represent typical household appliances commonly found in residential homes. Although these loads are common, their modern interfaces, which often include power electronics, and their ability to function as flexible loads required them to be reassessed in terms of their modelled characteristics. All the loads tested in this study fall under the Motor D, Power Electronic, or Static classifications of the CMPLDW model. At present, the CMPLDW model does not include an electric vehicle (EV) block. The testing of the home EV charger undertaken in this study provides valuable insights into the behaviour of EV loads and an indication of whether a separate EV block should be added to the CMPLDW model. Each device was brought to a steady operating condition before the disturbance was applied, and the operating point was held constant during the disturbance. The operating point was chosen to represent typical use or rated operation for the device, so that the pre-disturbance active and reactive power levels were stable and comparable across tests. EV charging tests were performed at the tested charging mode and level used in the experiments. These conditions define the baseline for the RMS trajectories reported in Sections 4 and 5. Variations in loading levels, e.g., during demand response modes or partial loading, were not included in this set of testing.

Table 6. Modern loads selected for tests.

Load Types
Refrigerators (conventional and inverter-based)
Heaters (electric fan and radiant)
Fans
Microwave Oven (inverter-based)
Air Conditioners (DOL and inverter-based)
Desktop (switch mode power supply)
Electric vehicle charger units
LED lights
Equipment with DOL motors (vacuum cleaner)

3.3. Laboratory Setup

The load testing procedure is depicted in Figure 2. To apply the disturbances, a California Instruments, San Diego, CA, USA, (MX45-3PI 45) arbitrary programmable power supply was employed. The load under examination was connected at the output of the power supply, and the voltage and current waveforms were measured at 10 kHz and processed using Matlab, Natick, MA, USA, to calculate the required active and reactive power responses of the devices. The Matlab program had the capability to calculate the Root Mean Square (RMS) variations in active power (P) and reactive power (Q) when subjected to changes in magnitude, frequency, and phase angle of the supply voltage. The analysis in this paper is focused on cycle-based RMS active and reactive power responses, consistent with RMS composite load modelling practice used for disturbance studies. The

10 kHz acquisition is not intended to fully resolve sub-cycle switching transients, but it provides sufficient resolution to compute RMS quantities accurately and to identify short duration behaviours that expose the limitations of cycle-based RMS representations. For electronically interfaced loads, fast effects such as inrush current and capacitor charging current motivate the use of EMT-based modelling for studies where sub-cycle behaviour is important, and the experimental results presented here provide a foundation for that subsequent work.

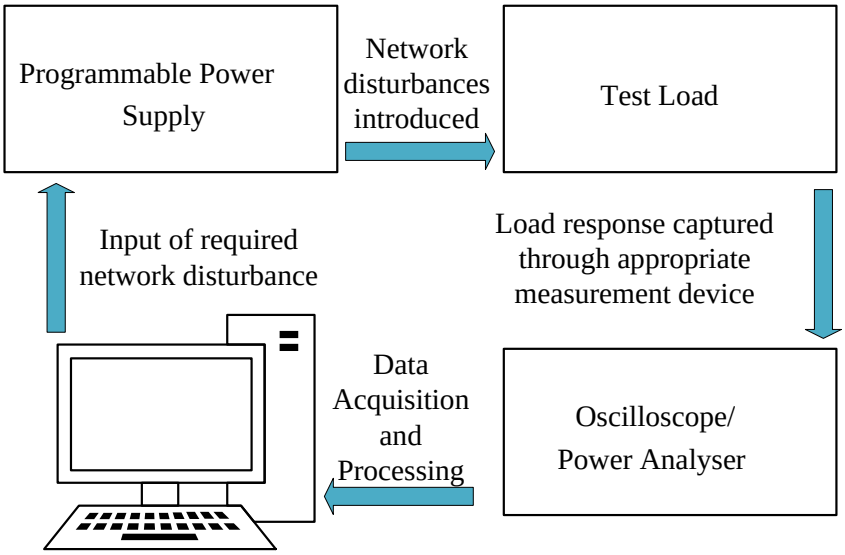


Figure 2. Schematic of experimental setup.

Figure 3 shows photographs of the laboratory setup. Figure 3a shows the programmable power supply utilised to apply the disturbances, while Figure 3b presents an example of an air conditioner load connected to the bench testing setup.



Figure 3. Load testing setup: (**a**) programmable power supply and (**b**) air conditioner under test.

4. Results

This section summarises the key results when the loads under test were subjected to the power system disturbances specified in Section 3. All the results presented in Sections 4 and 5 are derived from laboratory measurements and processed into RMS active and reactive power responses. The model description in Section 2 is provided as a reference framework to interpret the measured behaviours and inform parameter tuning in composite load studies; no simulation results are reported in this paper.

Considering the substantial number of tests conducted, the subsequent sections present only a summary of the most noteworthy results for each appliance. Additionally, detailed results for all the tests performed during this project have been shared with the Australian Energy Market Operator (AEMO) and are available on the project's dedicated website [19].

4.1. Refrigerators

Two refrigerators were evaluated. The first, Refrigerator 1, was an inverter-based unit, while the second, Refrigerator 2, was a conventional compressor unit. The purpose of including both types of refrigerators was to compare their responses to power system transients. According to the CMPLDW classifications, Refrigerator 1 was a motor D type load, which is known to be susceptible to stalling due to sags or undervoltage. In contrast, Refrigerator 2 was classified as an Electronic Load type.

For the voltage sag tests both refrigerators were found to be capable of riding through all of the applied disturbances. The only notable change during the transient period was a momentary variation in power consumption. Figure 4a,b depict the current waveforms of the two refrigerators when exposed to a voltage sag of magnitude 0.2 pu for a duration of 80 ms. The waveforms show that there is different dynamic response between the two devices. After the sag was cleared, both devices experienced an overshoot in current. For Refrigerator 1, the overshoot was due to the d.c. side capacitor charging to its nominal value (characterised by a very short-term high magnitude current value), while for Refrigerator 2, it was due to motor inrush current (characterised by longer-term decaying current magnitudes). The duration of the sags applied had no notable impact on the response of the devices.

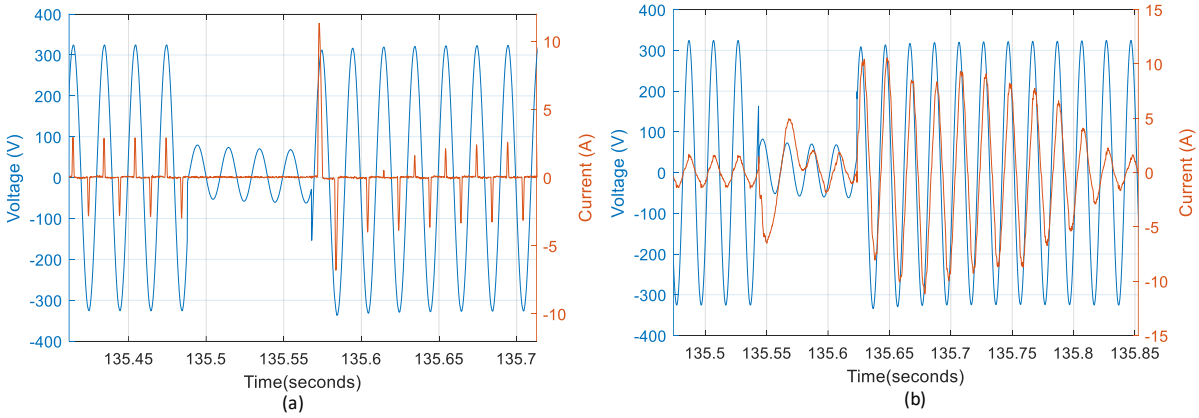


Figure 4. Impact of voltage sag on (**a**) Refrigerator 1 and (**b**) Refrigerator 2.

During the voltage swell tests, both refrigerators were able to withstand the voltage swells without any disconnection. The only change observed during the transient period was a temporary variation in the current drawn by the devices. A total of 18 voltage swell disturbances were applied, with the maximum applied voltage magnitude being 1.2 pu. Neither device experienced any disruption in normal operation once the swells were cleared.

During the phase angle jump tests, the conventional compressor system in Refrigerator 2 stalled when the phase angle magnitude was $-90°$, causing an increase in active power consumption from 100 W to approximately 1200 W while the reactive power absorption increased from 45 VAr to 1000 VAr. The device remained in the stalled state for several minutes before returning to normal. There was no impact on Refrigerator 2 for all other phase angle jumps with an angle of less than 90°. The performance of the inverter-based refrigerator (Refrigerator 1) was not impacted by any of the applied phase angle jumps. The response of

the currents drawn by Refrigerator 1 and Refrigerator 2 during a phase angle jump of −90° are shown in Figure 5a and Figure 5b, respectively.

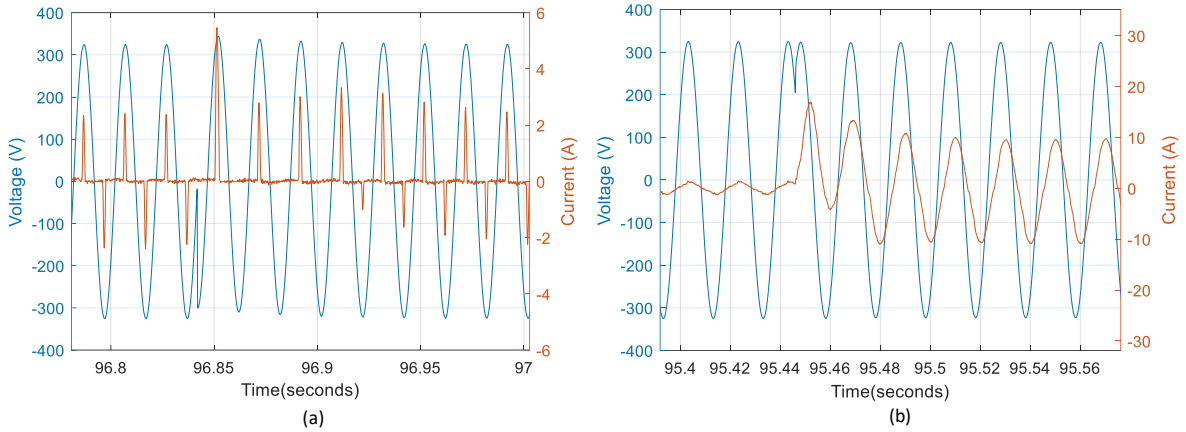


Figure 5. Impact of phase angle jumps on (**a**) Refrigerator 1 and (**b**) Refrigerator 2.

4.2. Microwave Oven

This section presents the response of an inverter-based microwave oven. This device had a steady-state active power consumption of 1050 W and a capacitive reactive power injection of 180 VAr.

Figure 6 shows the variation of the active and reactive power during a voltage sag with a retained voltage of 0.2 pu and a swell event where the voltage was increased to 1.2 pu. During the sag, the device experienced momentary cessation, while during the swell, the active power consumption increased to 1250 W and the reactive power changed from −180 VAr to +900 VAr. After the disturbance was cleared, the device returned to its steady-state operation without any significant peaks in either the real or reactive power. Similar responses were recorded for all other sag and swell tests.

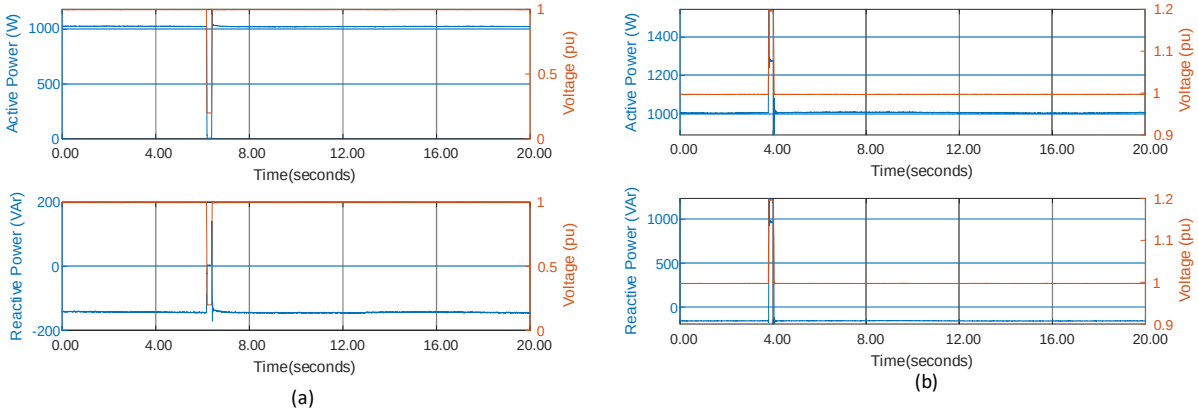


Figure 6. Response of microwave oven load when subject to a sag/swell with a duration of 220 ms: (**a**) a sag with a magnitude of 0.2 pu, and (**b**) a swell with a magnitude of 1.2 pu.

The microwave oven exhibited some interesting characteristics during frequency disturbance tests, despite not being expected to exhibit any changes in active and reactive power based on the CMPLDW definition for an electronic load. Figure 7 shows that a change in frequency caused the active power consumption of the device to vary in a linear manner for both step and ramp frequency changes. The same behaviour was observed for reactive power. Figure 7a–d depict the changes in active power consumption of the device during step changes in the supplied voltage frequency from 50 to 52 Hz, 50 Hz to 47 Hz, and ramp frequency changes of +0.4 Hz/s and −0.4 Hz/s, respectively. The device

operated without any significant variation in its power characteristics for all phase angle jump tests.

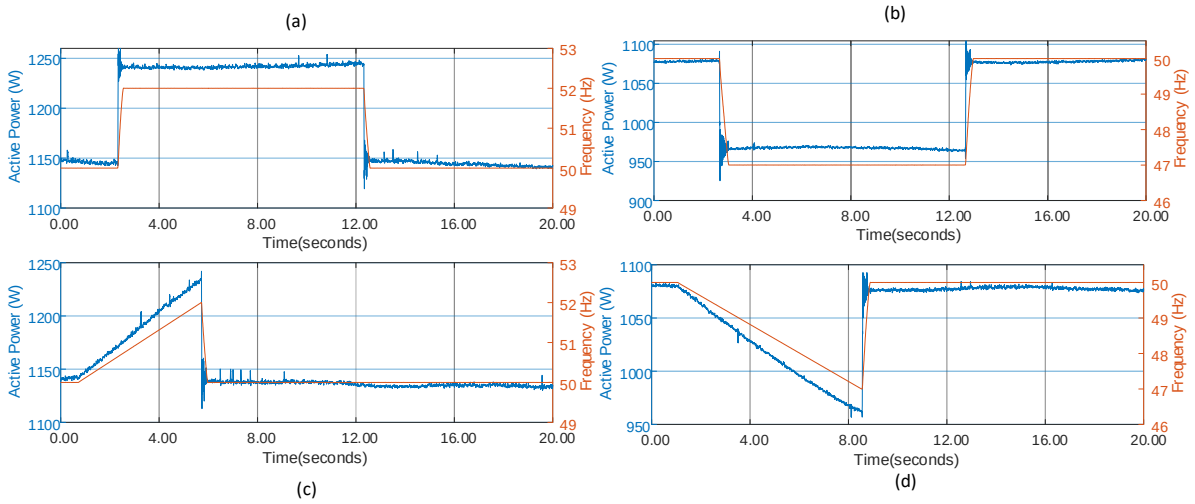


Figure 7. Frequency change responses of the microwave oven with (**a**) a step change from 50 Hz to 52 Hz and (**b**) 50 Hz to 47 Hz, (**c**) a ramp of +0.4 Hz/s, and (**d**) a ramp of −0.4 Hz/s.

4.3. Air Conditioners

4.3.1. DOL Conventional Unit

This section of the paper summarises the outcomes of the test results for a portable air conditioner. This device had a power consumption of approximately 1 kW and draws 100 VAr during steady state conditions. The air conditioner was set to the maximum cooling setting during testing. This device was categorised as a Motor D type in CMPLDW and as such may be susceptible to stalling in the event of power system faults.

For all sag and swell tests, except for the sag with a retained voltage of 0.2 pu (the lowest), the air conditioning returned to its normal operating condition when voltage returned to nominal. However, in the case of the sag with a retained voltage of 0.2 pu, the compressor motor stalled for a brief period and the cooling system turned off. The motor then resumed operation after approximately 30 s. Figure 8a demonstrates the stall characteristics of the air conditioner during a sag with a voltage reduction to 0.2 pu for 220 ms. This behaviour was also observed for sags of different durations at the same magnitude. Figure 8b shows the response of the device when subjected to a swell for 220 ms, where the voltage was increased to 1.2 pu. Here it can be seen that the impact of the swell was a momentary change in both the active and reactive power.

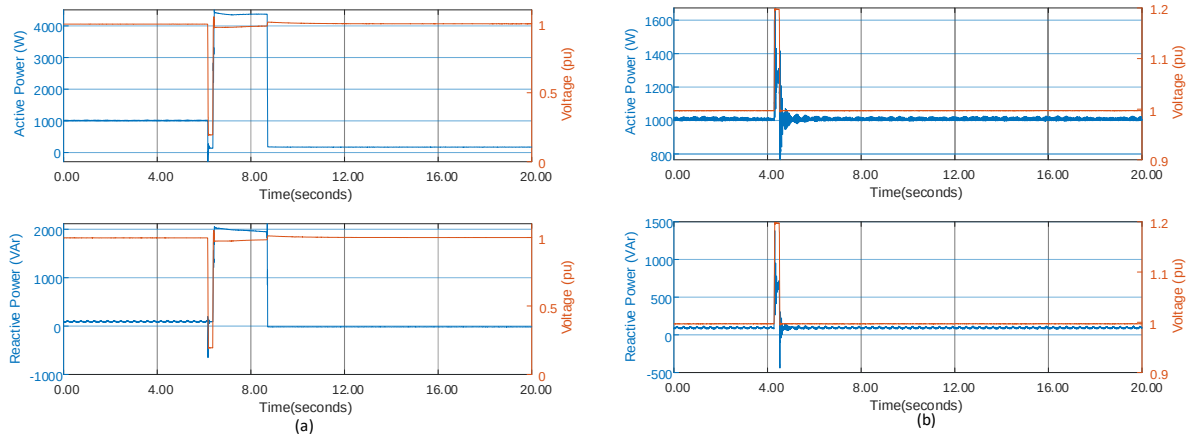


Figure 8. Response of the air conditioner when subject to voltage disturbances: (**a**) sag and (**b**) swell.

The air conditioner experienced brief fluctuations in active power in response to both step and ramp changes in frequency. However, the reactive power consumption varied inversely with the frequency change. Figure 9 presents the active and reactive power responses of the device to step changes in frequency. The graph indicates that the reactive power consumption increased from 100 VAr to 300 VAr when the frequency was reduced from 50 Hz to 47 Hz, and the reactive power consumption decreased to zero when the frequency was increased from 50 Hz to 52 Hz. Similar behaviour was observed in the reactive power characteristics for ramp changes in frequency.

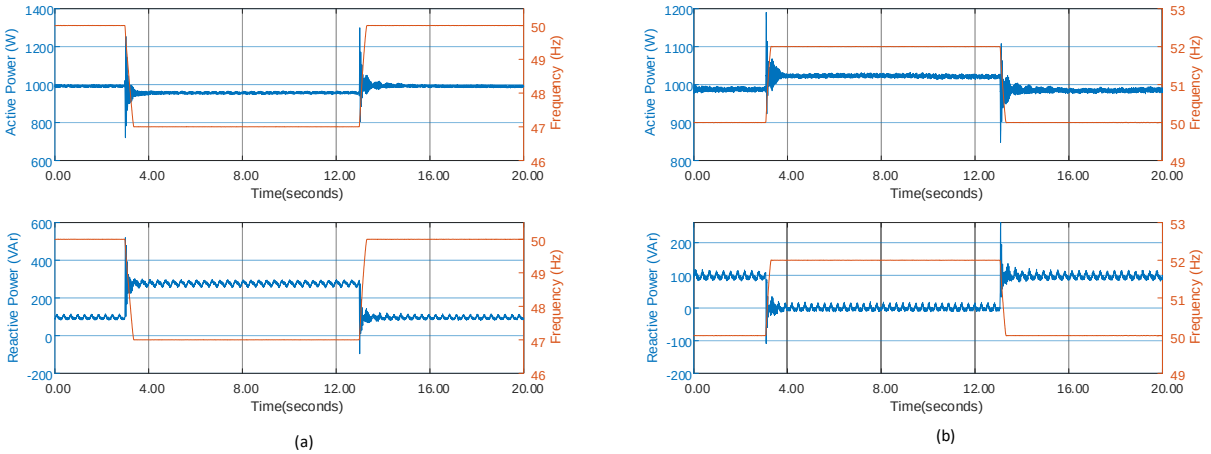


Figure 9. Frequency change responses for the air conditioner: (**a**) a step decrease to 47 Hz and (**b**) a step increase to 52 Hz.

Regarding phase angle jumps, the air conditioner only experienced brief changes in both the active and reactive power for phase angle magnitudes below 90°. However, for a voltage phase shift of 90°, the device was not impacted by the +90° shift but appeared to stall when subjected to a phase shift of −90°. The active and reactive power variations when the device was subjected to the 90° phase shift disturbance are shown in Figure 10a. The graph depicts an increase in both the active and reactive power as the motor stalls for approximately 3 s. During the stalled operation, the active power increased to 4500 W and the reactive power increased to over 2000 VAr. Figure 10b illustrates how the current drawn by the unit varies, and it is evident that the current drawn during the period where it appeared to be stalled is significantly higher than during steady-state operation.

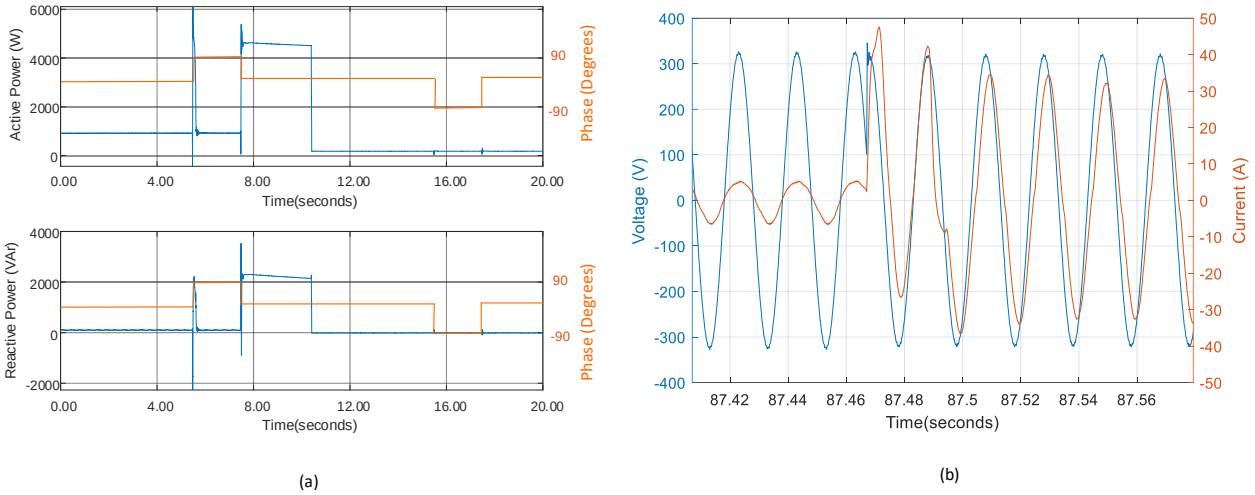


Figure 10. Impact of a phase angle jump on air conditioner operation: (**a**) P and Q response and (**b**) current drawn.

4.3.2. Inverter-Based Units

This section presents the results obtained from testing three residential inverter-based split-system air conditioner units. It is important to note that these units differ from the direct-on-line (DOL) unit studied in Section 4.3.1, as they are classified as electronic load devices. Unlike DOL units, inverter-based units employ power electronic control algorithms to increase efficiency. The three units tested have been termed Air Conditioner 1, Air Conditioner 2, and Air Conditioner 3.

For the voltage sag tests, in contrast to the DOL air conditioner, which exhibited stalling behaviour, the inverter-based units did not experience any stalling issues across the range of voltage sag scenarios evaluated. However, the units did cease operation for longer, deeper sags. Tables 7–9, representing Air Conditioner 1, Air Conditioner 2, and Air Conditioner 3, respectively, provide indications of the voltage sag magnitudes that caused the devices to either continue operating normally or cease operation. It is evident that Air Conditioner 1 was able to continue operating if the voltage magnitude remained above 0.4 pu. In the case of Air Conditioner 2, the unit ceased operation for sags with a duration of 220 ms and when the voltage magnitude dropped to 0.5 pu or lower. For Air Conditioner 3, the unit ceased operation for sags of any duration as soon as the retained voltage was 0.4 pu or lower.

Table 7. Summary of voltage sag tests for Air Conditioner 1.

Sag Duration	Voltage Amplitude (pu)							
	0.9	**0.8**	**0.7**	**0.6**	**0.5**	**0.4**	**0.3**	**0.2**
80 ms	✓	✓	✓	✓	✓	✓	×	×
120 ms	✓	✓	✓	✓	✓	✓	×	×
220 ms	✓	✓	✓	✓	✓	✓	×	×

Note: ✓ = ride-through; × = disconnection.

Table 8. Summary of voltage sag tests for Air Conditioner 2.

Sag Duration	Voltage Amplitude (pu)							
	0.9	**0.8**	**0.7**	**0.6**	**0.5**	**0.4**	**0.3**	**0.2**
80 ms	✓	✓	✓	✓	✓	✓	✓	✓
120 ms	✓	✓	✓	✓	✓	✓	✓	✓
220 ms	✓	✓	✓	✓	×	×	×	×

Note: ✓ = ride-through; × = disconnection.

Table 9. Summary of voltage sag tests for Air Conditioner 3.

Sag Duration	Voltage Amplitude (p.u)							
	0.9	**0.8**	**0.7**	**0.6**	**0.5**	**0.4**	**0.3**	**0.2**
80 ms	✓	✓	✓	✓	✓	×	×	×
120 ms	✓	✓	✓	✓	✓	×	×	×
220 ms	✓	✓	✓	✓	✓	×	×	×

Note: ✓ = ride-through; × = disconnection.

These results indicate that each unit has its own distinct control and protection mechanism, which leads to variations in behaviour. Another interesting observation from these results is that Air Conditioner 3 had a delay after the voltage sag before it ceased operation. In comparison, Air Conditioner 1 and Air Conditioner 2 ceased operation as soon as the sag disturbance was applied.

With respect to voltage swell tests, all air conditioners did not appear to be impacted. The responses of Air Conditioner 1, Air Conditioner 2, and Air Conditioner 3 during a voltage swell test, where the voltage was increased to 1.2 pu for 80 ms, are shown in Figure 11a, Figure 11b, and Figure 11c, respectively. The plots clearly illustrate that during the swell event, there is a brief spike in current, which can be attributed to the charging of the capacitors within the units. However, once the voltage returned to normal, the devices resumed their normal operation, as indicated by the subsequent plots. Similar responses were observed for the other voltage swell tests, indicating the ability of these inverter-based air conditioners to effectively ride through such disturbances without any adverse effects.

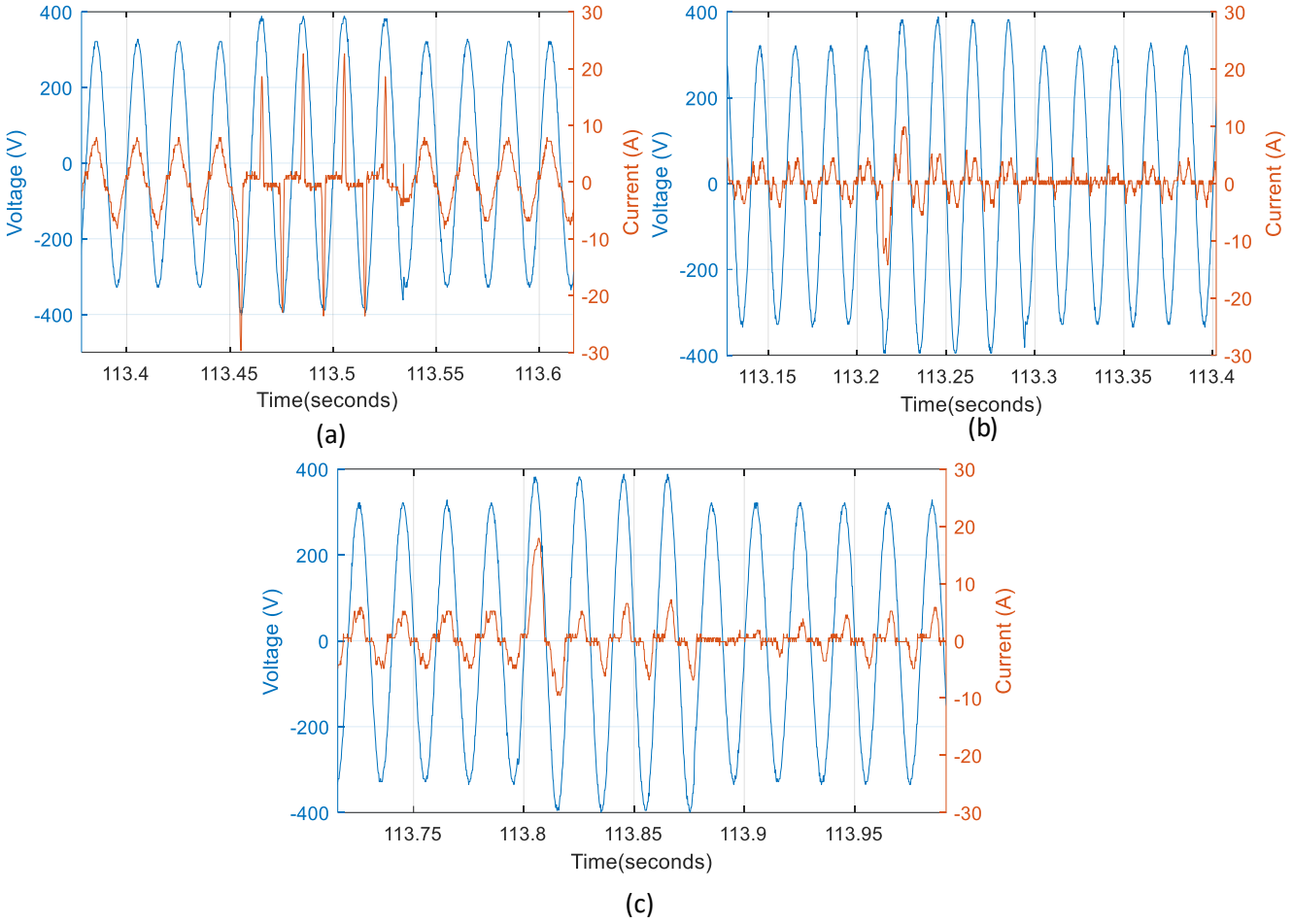


Figure 11. Response to a swell of voltage magnitude of 1.2 pu for 80 ms: (**a**) Air Conditioner 1, (**b**) Air Conditioner 2, and (**c**) Air Conditioner 3.

In relation to frequency and phase angle jump disturbances, the inverter-driven air conditioners maintained normal operation throughout all the tests. An example of this can be seen in Figure 12a, which showcases the response of Air Conditioner 1 to a frequency step change from 50 Hz to 47 Hz. This consistent behaviour was observed across all frequency tests conducted on the three air conditioners. Additionally, Figure 12b displays the current waveform of Air Conditioner 1 during a -90° phase angle jump, where no significant impact is evident as the current continues its regular operation following the phase jump in the voltage waveform. Once again, all three devices exhibited similar responses.

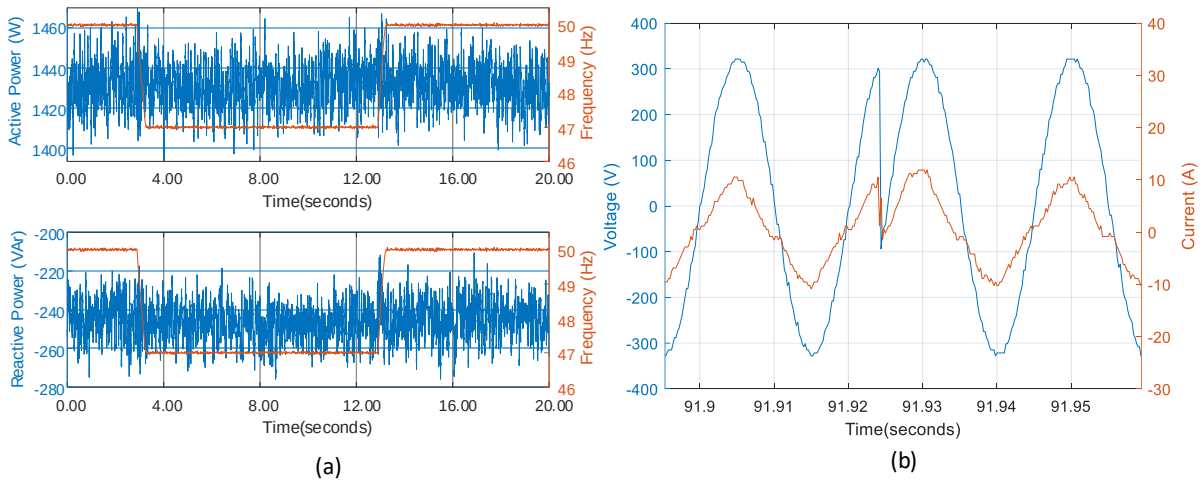


Figure 12. (**a**) Impact of step frequency disturbance on Air Conditioner 1, and (**b**) impact of −90° phase angle jump on Air Conditioner 1.

4.4. Motor-Based Appliances

4.4.1. Vacuum Cleaner

This section presents the test results for a vacuum cleaner. The appliance had a power rating of 2 kW, and during the tests conducted at maximum power, it consumed 1.6 kW of active power and 100 VAr of reactive power. This resulted in a lagging power factor of 0.998.

Figure 13a illustrates the response of the device during the voltage sag test where the retained voltage was 0.2 pu. Figure 13b depicts the response for both the active power (P) and reactive power (Q) when the voltage was increased to 1.2 pu, representing the maximum voltage swell test. It is evident from the figures that the device was able to resume normal operation once the disturbances were complete.

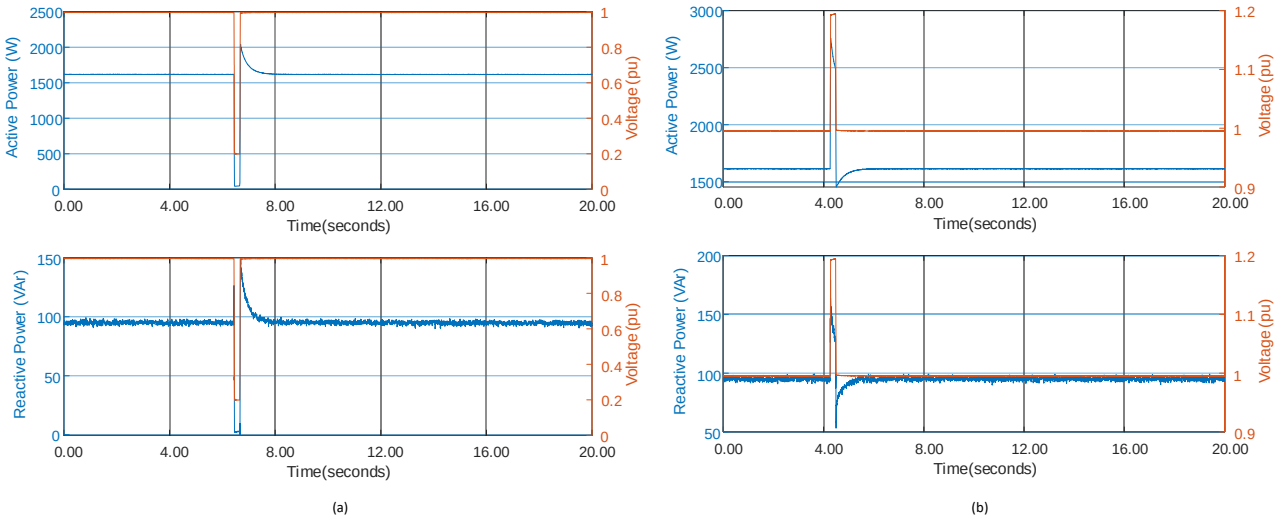


Figure 13. Response of the vacuum cleaner to (**a**) a sag with a retained voltage of 0.2 pu for 220 ms, and (**b**) a swell with a voltage of 1.2 pu for 220 ms.

As the vacuum cleaner is a motor-based device, the transient overshoot in the real and reactive power responses indicates the inrush currents associated with the motor's operation.

During the frequency tests, the vacuum cleaner exhibited no significant changes in its active power consumption, with only minor variations observed in the reactive power. Figure 14a displays the response when the frequency is reduced from 50 Hz to 47 Hz at a rate of 0.4 Hz/s, revealing a reduction in reactive power from approximately 100 VAr to approximately 90 VAr.

In Figure 14b, which shows the results of a step frequency change test, the reactive power consumption increases from 100 VAr to approximately 105 VAr. For all frequency tests, the reactive power levels returned to their nominal value once the nominal frequency was restored. For phase angle jump disturbances, the vacuum cleaner's current waveform experienced a phase angle jump without any overshoot at the time of the disturbance.

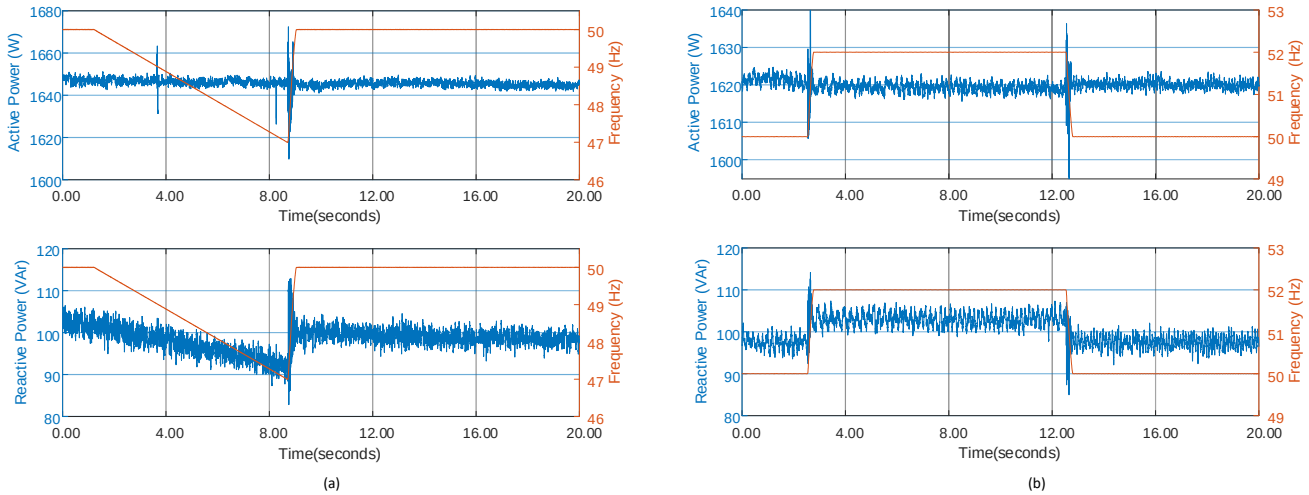


Figure 14. Frequency response of the vacuum cleaner with (**a**) a reduction in frequency at 0.4 Hz/s, and (**b**) a step increase in frequency from 50 Hz to 52 Hz.

4.4.2. Fan

This section provides a summary of the test results obtained for a pedestal fan. Under normal operating conditions, the fan consumed approximately 75 W of active power with a capacitive reactive power of −12 VAr.

During voltage sag and swell disturbances, the fan experienced momentary changes in both active and reactive power consumption. Figure 15a illustrates the reduction in both active and reactive power levels for the fan during a sag event, where the voltage was reduced to 0.2 per unit (pu) for 220 ms. Figure 15b demonstrates how the active and reactive power of the fan increased during the swell event.

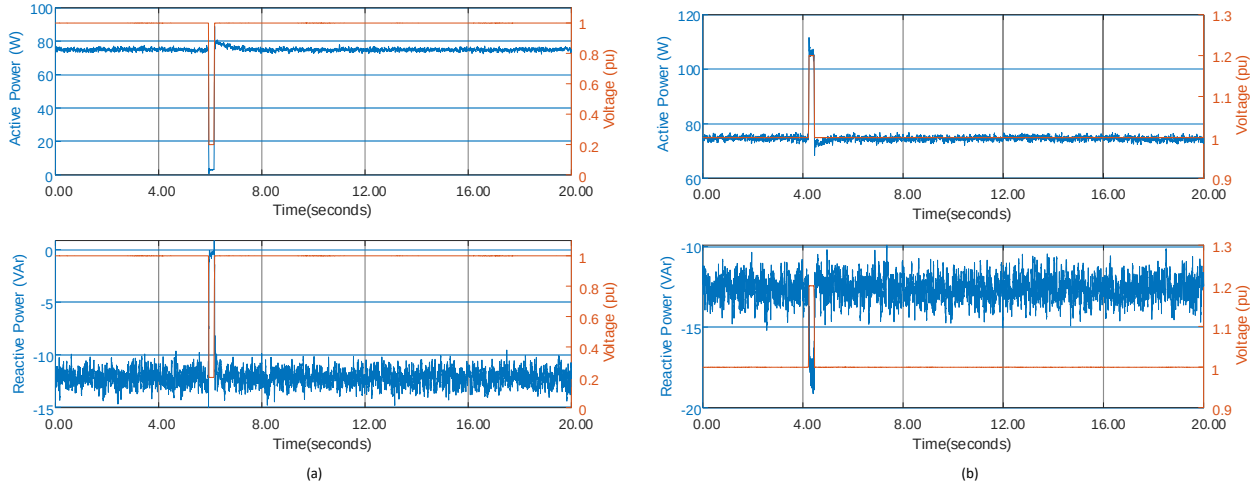


Figure 15. Response of fan for voltage sag and swell disturbances of (**a**) 0.2 pu sag for 220 ms, and (**b**) 1.2 pu swell for 220 ms.

In the sag test, the active power consumption of the fan dropped to 3 W from 75 W, while during the swell, the active power increased to approximately 107 W. This behaviour

indicates that the fan response is similar to that of a constant impedance load, where the power consumption is proportional to the square value of the applied voltage.

After the disturbances were complete, the fan returned to its normal operating conditions, albeit with a small inrush current overshoot, which is typical for such motor-based devices.

For frequency disturbances, the active and reactive power levels of the fan exhibited a proportional change to the applied frequency of the power supply. Figure 16a illustrates the variations in active power (P) and reactive power (Q) when the frequency was decreased from 50 Hz to 47 Hz, while Figure 16b depicts the corresponding changes when the frequency was increased from 50 Hz to 52 Hz.

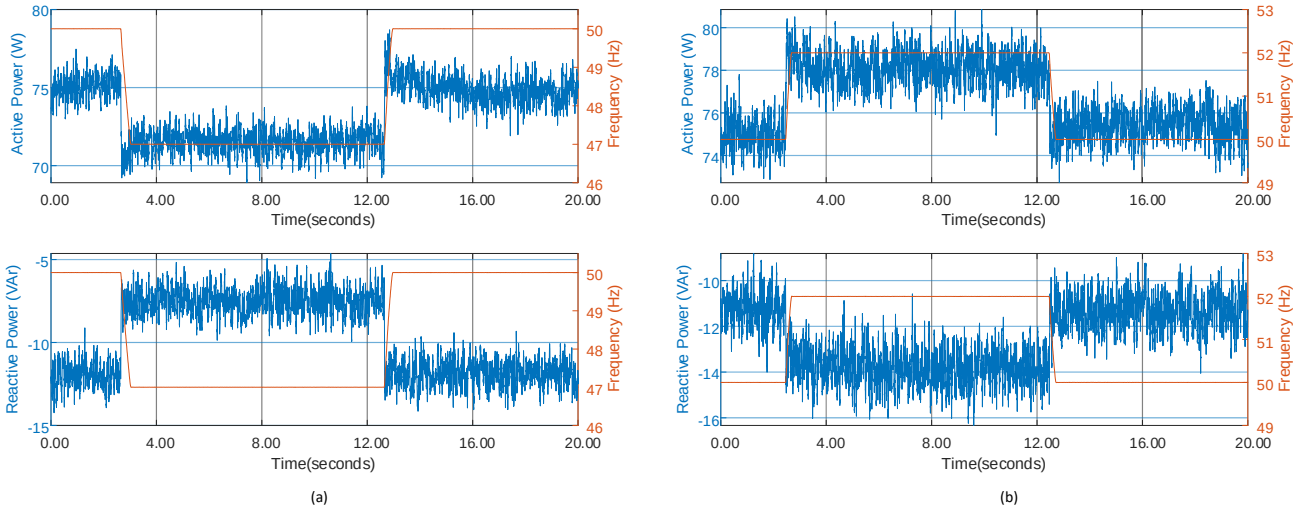


Figure 16. Frequency response of the fan with (**a**) a step decrease in frequency from 50 Hz to 47 Hz, and (**b**) a step frequency from 50 Hz to 52 Hz.

During the frequency decrease, the active power consumption of the fan decreased from 75 W to 72 W, while for the frequency increase, the fan's power consumption increased to approximately 78 W. These results indicate that the fan's power consumption responds in accordance with the changes in the supplied frequency. Similar behaviour was observed for the ramp frequency disturbances applied during the tests. The fan did not exhibit any significant changes in its active and reactive power consumption during the phase angle jump tests.

4.5. Heaters

In this section, the results of the tests conducted on two common types of heaters, Heater 1, a radiant coil-based heater, and Heater 2, an air-forced heater, are presented. Under steady-state conditions, Heater 1 consumes 1200 W of active power and has a reactive power of −20 VAr, while Heater 2 consumes 800 W of active power with an inductive reactive power of +10 VAr.

Following a voltage sag event, both heaters displayed a temporary reduction in power consumption. Figure 17a illustrates the active power (P) and reactive power (Q) response of Heater 1, while Figure 17b demonstrates the P and Q response of Heater 2 when subjected to a voltage sag with a retained voltage of 0.2 pu for a duration of 220 ms. Once the voltage returned to its nominal value, both heaters returned to their normal power consumption levels.

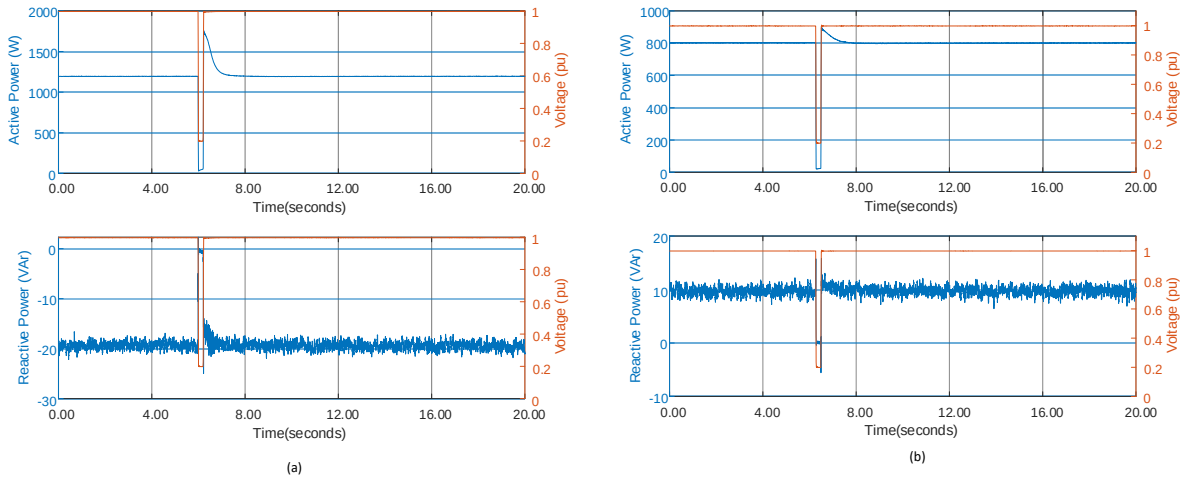


Figure 17. Heater response to sag of a retained voltage magnitude of 0.2 pu for 220 ms: (**a**) Heater 1 and (**b**) Heater 2.

During the recovery phase, a short transient overshoot in current was observed for both heaters. In the case of Heater 1, the transient overshoot may be attributed to the re-energising of the heating coils. As for Heater 2, the overshoot could be attributed to inrush currents resulting from the fan motor.

The responses of the heaters during voltage swell tests were similar to that observed for voltage sag tests. As the voltage increased during the swell, there was a corresponding increase in power consumption, and once the swell event concluded, the heaters returned to their normal operating conditions. This behaviour was observed across all swell tests.

Regarding frequency changes, no noticeable effects were observed on the heaters. Figure 18a illustrates the impact on the active power (P) and reactive power (Q) of Heater 1 during a gradual frequency change from 50 Hz to 47 Hz at a rate of 0.4 Hz/s. Similarly, Figure 18b displays the response of Heater 2 to the same frequency disturbance. In both cases, there were no significant changes in the power consumption of the heaters. Furthermore, the voltage phase angle tests did not appear to have any significant impact on heater operation.

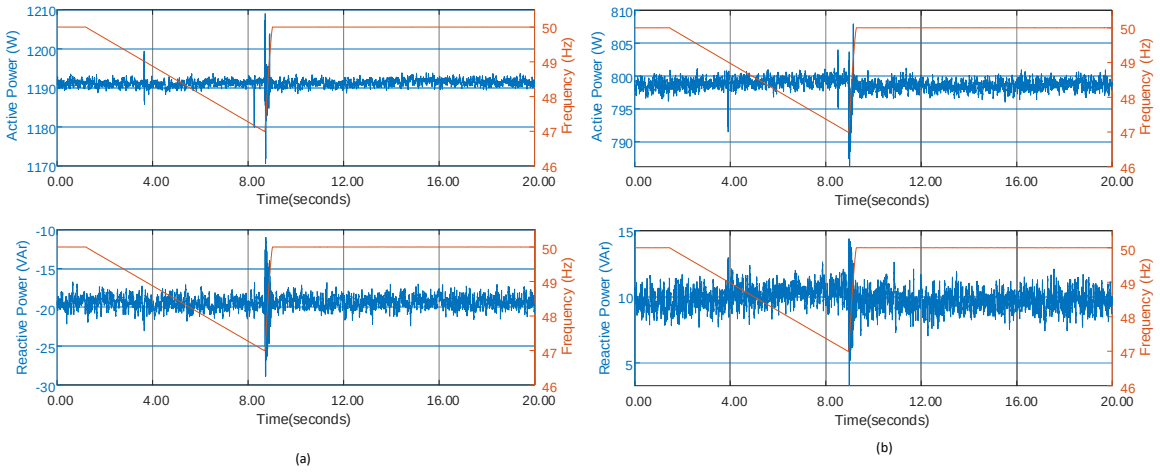


Figure 18. Impact of frequency disturbance: (**a**) Heater 1 and (**b**) Heater 2.

4.6. LED Lighting

This section presents the results of testing for an LED lamp. Under normal operating conditions, the LED bulb consumed 10 W of active power with a capacitive reactive power of −5 VAr. During the voltage sag tests, the bulb experienced a momentary cessation of

light output for all sags when the voltage dropped below 0.7 pu retained voltage. However, when the voltage remained above 0.7 pu, as shown in Figure 19a, the LED bulb exhibited no significant changes in its active and reactive power levels.

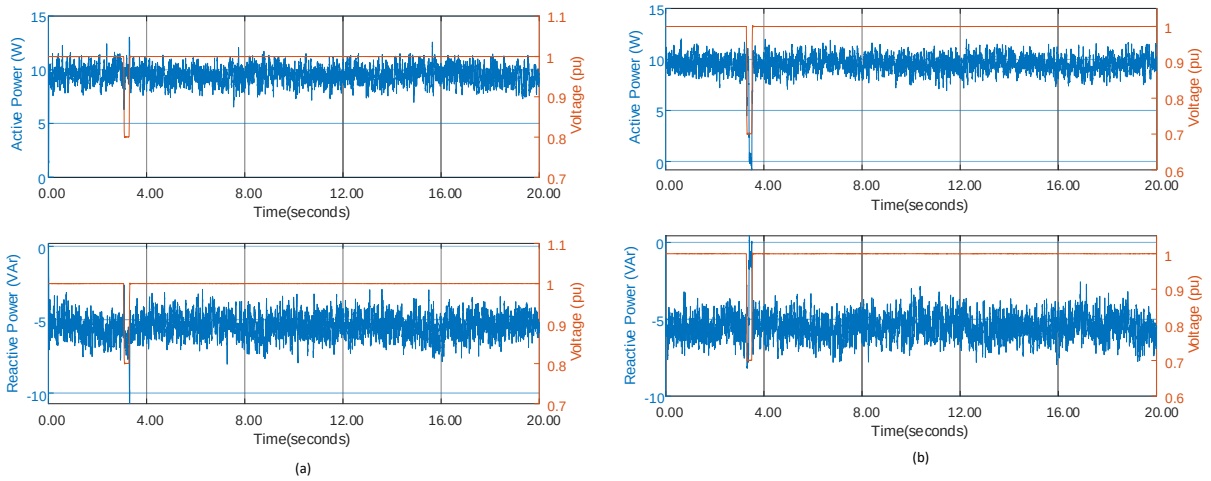


Figure 19. Response of the LED light bulb for a voltage sag of duration 220 ms with a retained voltage magnitude of (**a**) 0.8 pu and (**b**) 0.7 pu.

For all voltage sags where the magnitude of the voltage fell below 0.7 pu, both the active and reactive power of the LED bulb reduced to zero during the sag event. An example of this is plotted in Figure 19b, when the voltage was dropped to 0.7 pu during the sag disturbance. This phenomenon was also visually observed through the flickering of the LED bulb during the testing. These results indicate that the LED light bulb is sensitive to voltage sags, and its performance is affected when the voltage drops below a certain threshold.

Other tests conducted on the LED light bulb, including voltage swells, frequency changes, and phase angle jumps, did not result in any significant changes in both the active and reactive power levels of the device.

Figure 20a presents the active and reactive power values for the LED bulb when subject to a voltage swell with a magnitude of 1.2 pu for a duration of 220 ms. The graph demonstrates that the LED bulb maintained stable active and reactive power levels throughout the voltage swell event. Similarly, Figure 20b illustrates the response of the LED bulb during a step frequency change from 50 Hz to 52 Hz. In this test, the LED bulb exhibited no notable variations in its active and reactive power consumption.

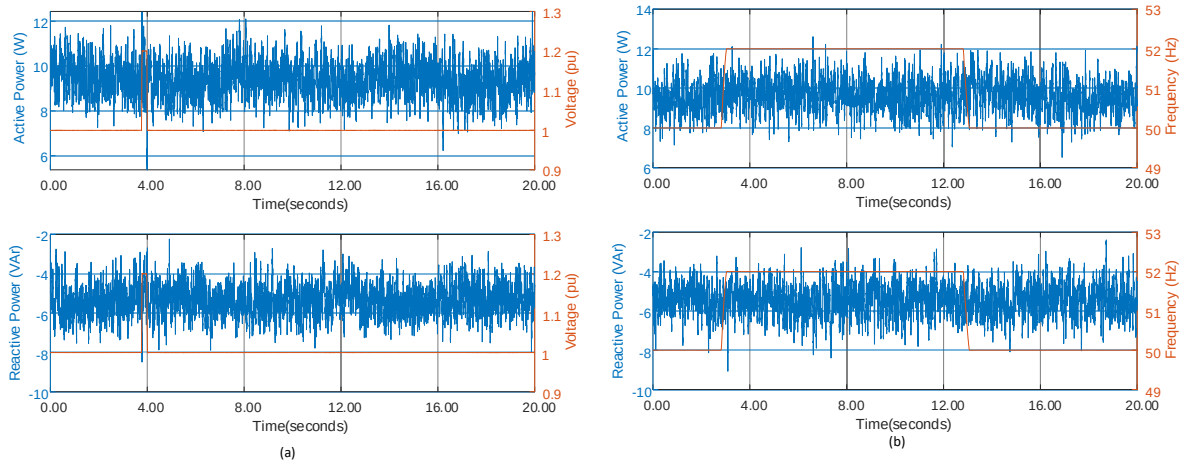


Figure 20. Response of the LED light bulb during a (**a**) voltage swell of 1.2 pu for 220 ms, and (**b**) step frequency increase from 50 Hz to 52 Hz.

5. EV Charger Units

5.1. Level 1 EV Charging Unit

This section summarises the results of bench testing for a home electric vehicle (EV) charger. The charger tested is a Level 1 AC charger supplied with a Type 1 EV connector. During normal operation, the device consumed 2200 W of active power with a power factor of 0.93 leading. To ensure consistency, the State of Charge (SoC) of the EV was kept below 80% for all the tests. The EV testing in this paper is included to demonstrate that EV charging can exhibit distinct disconnection and reconnection behaviours under disturbances. These behaviours can be important for composite load studies as EV penetration increases. Development of a dedicated EV charger model block is outside the scope of this paper.

The EV charger was able to ride through voltage sags of all durations if the retained voltage was above 0.6 pu. Figure 21a displays the instantaneous current response of the EV charger during a 220 ms sag with a retained voltage magnitude of 0.6 pu. The current stabilises to its original value after an initial sag transient overshoot, indicating that the charger has the characteristics of a constant current device. Once the fault is cleared, the current drawn decreases briefly before returning to its nominal value. Figure 21b shows the RMS active and reactive power response of the EV during the same voltage sag. Both the active and reactive power decrease during the sag, while the charger continues to charge the EV once nominal voltage is restored.

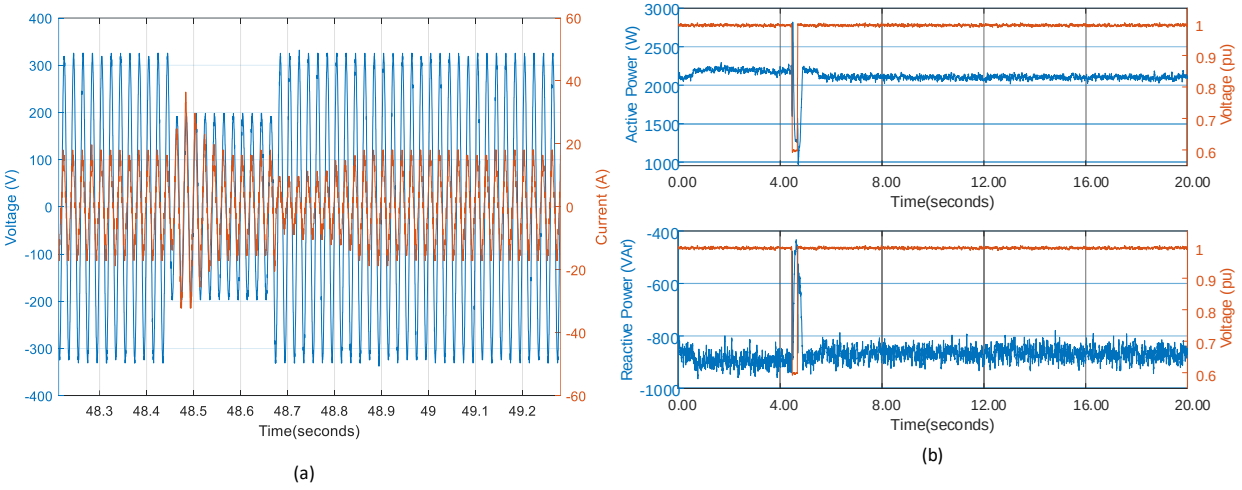


Figure 21. Response of the EV Charger to a sag of 0.6 pu for 220 ms: (**a**) voltage–current response and (**b**) PQ response.

If the retained voltage magnitude was 0.5 pu or less, the EV charger disconnected from the vehicle by opening the contactor in the device. It was observed that in this case, the charger remained disconnected for a period before ramping up to its nominal charging power. Interestingly, two sets of reconnection times were recorded when the depth of the voltage sag was varied. Figure 22a,b illustrate the charger's responses when subjected to sags with retained voltage magnitudes of 0.4 pu and 0.3 pu, respectively.

Table 10 summarises the response and reconnection times of the tested EV charger when exposed to sags of different durations and magnitudes.

Table 10. Response of EV charger for voltage sags of different magnitudes and durations.

Voltage Sag	0.8 pu	0.7 pu	0.6 pu	0.5 pu	0.4 pu	0.3 pu	0.2 pu
80 ms	Ride Through	Ride Through	Ride Through	Ride Through	Ride Through	Disconnect for 32 s	Disconnect for 32 s
120 ms	Ride Through	Ride Through	Ride Through	Disconnect for 7 s	Disconnect for 7 s	Disconnect for 32 s	Disconnect for 32 s
220 ms	Ride Through	Ride Through	Ride Through	Disconnect for 7 s	Disconnect for 7 s	Disconnect for 32 s	Disconnect for 32 s

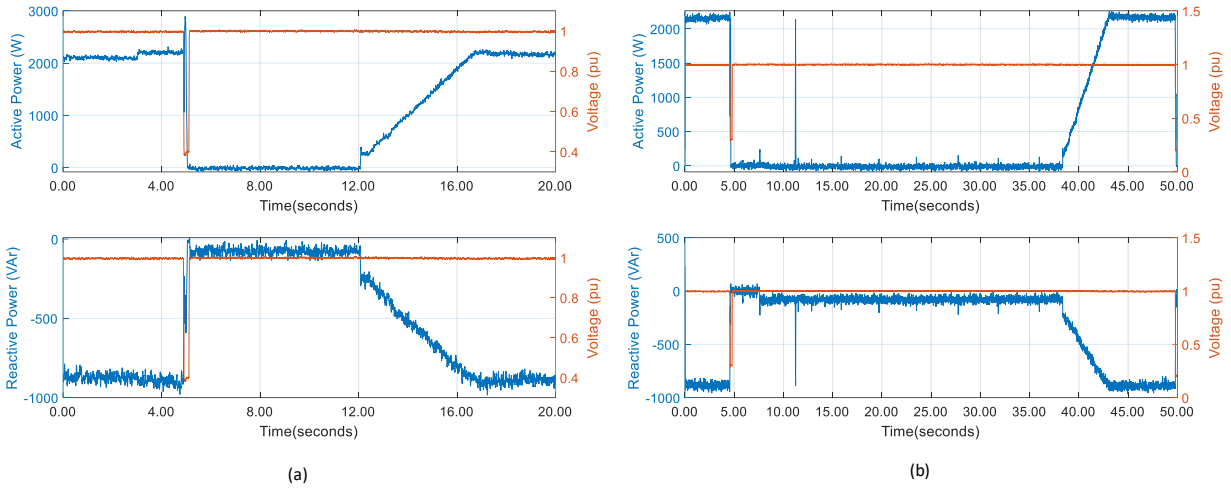


Figure 22. Demonstration of different reconnection times depending on the retained voltage during a voltage sag of (**a**) 0.4 pu and (**b**) 0.3 pu.

The EV charger did not appear to be significantly impacted during the voltage swell tests. There was a temporary rise in both the active and reactive power of the charger. Frequency changes, whether in step or ramp form, did not result in any significant impact on the charger. Figure 23a,b depict the charger's response to a step frequency change from 50 to 52 Hz and the active and reactive power consumption during a ramp frequency change from 50 Hz to 47 Hz at a rate of −4 Hz/s, respectively. During the testing of response to voltage phase angle jumps, no noticeable change was observed in its operation, and no disconnection occurred. The current waveform experienced a phase angle jump without any overshoot at the time of the disturbance.

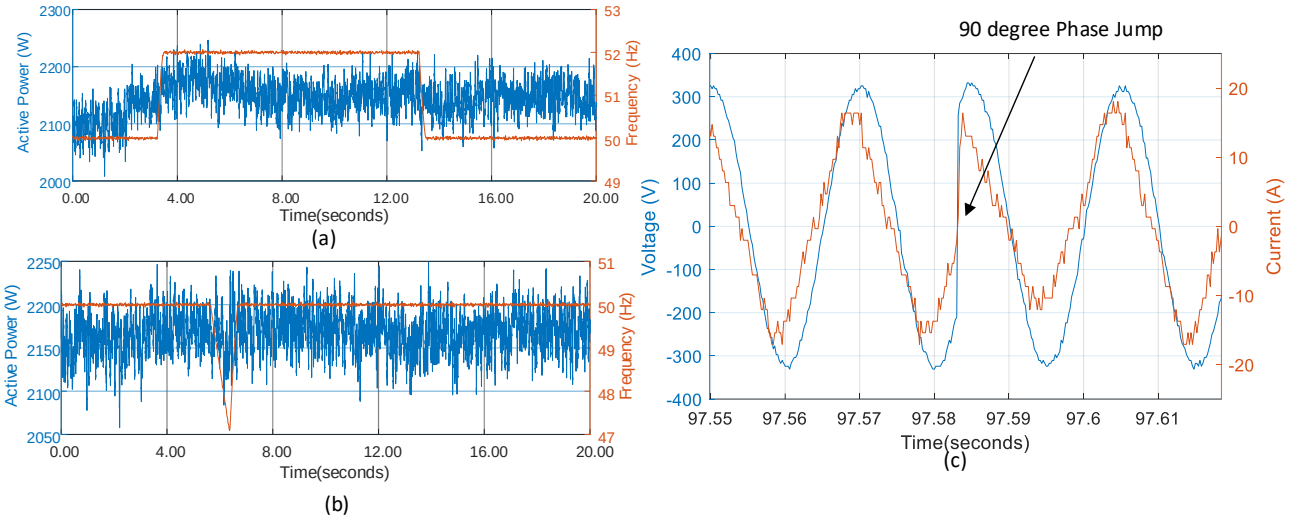


Figure 23. Impact of frequency changes and phase angle jumps for the EV charger: (**a**) step frequency change from 50 Hz to 52 Hz, (**b**) ramp frequency at −4 Hz/s, and (**c**) phase angle jump.

5.2. Level 2 EV Charger

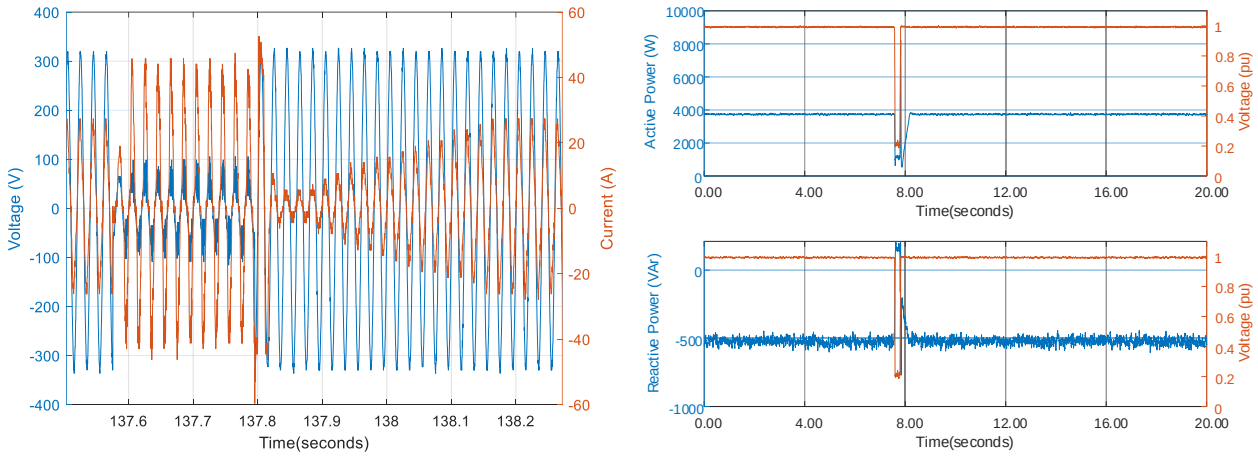
This section presents a summary of the results obtained from the testing of a Level 2 electric vehicle (EV) charger, commonly found in commercial car parks and residential homes. The tested charger has a rated power of 7.4 kW; however, the actual power drawn during testing was approximately 3.7 kW. This discrepancy is attributed to the power limitations of the EV model tested (Nissan Leaf 2012). Under normal operating conditions, the charger consumed 500 VAr of reactive power, resulting in a leading power factor of 0.99. Similar to the case for the level 1 EV charger, the EV's State of Charge was maintained

to below 80% throughout all testing. Figure 24 shows a photograph of the EV charging setup used to perform these tests.



Figure 24. Photograph of EV charger test setup.

For voltage sag disturbances, the charger successfully rode through all applied sags. Figure 25 illustrates the charger response when subjected to a sag with a voltage depth of 0.2 pu retained voltage for a duration of 220 ms. Figure 25a displays the instantaneous current and voltage waveforms during the sag, while Figure 25b displays the active and reactive power responses. Both the active and reactive power experience a momentary decrease during the sag; however, the charger resumes charging the EV once the nominal voltage is restored.



(**a**) (**b**)

Figure 25. Response of the EV charger to a voltage sag of 0.2 pu retained voltage for 220 ms: (**a**) current response and (**b**) P and Q response.

For the voltage swell tests, the EV charger operated without any interruption. Figure 26a displays the current response of the EV charger during a swell, when the voltage was momentarily increased to 1.2 pu for a duration of 220 ms. During the swell, the charger current draw decreased, indicating a response like that of a constant power load.

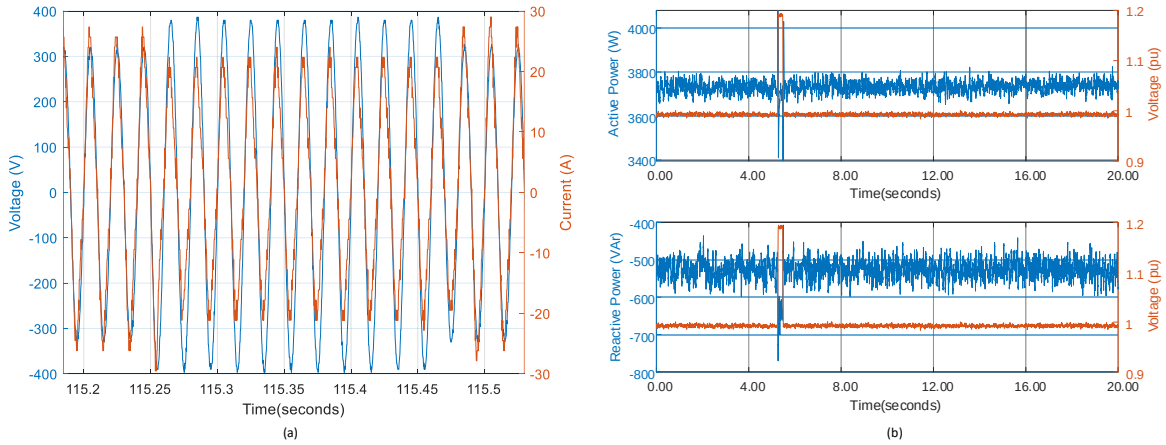


Figure 26. EV charger response to a voltage swell of magnitude 1.2 pu for 220 ms: (**a**) current response and (**b**) P and Q response.

The response of the charger's real and reactive power during a voltage swell test is depicted in Figure 26b, illustrating an ability to ride through the disturbance with only minor transient oscillations. Once the voltage swells were cleared, the charger promptly resumed normal operation.

During the frequency disturbance tests, the EV charger showed no significant changes in active and reactive power levels, consistent with the definition of an electronic load as per the CMPLDW. Figure 27a,b illustrate the P and Q response of the EV charger when subjected to a step frequency change from 50 Hz to 47 Hz and 52 Hz, respectively. There is no discernible change in either the active or reactive power values. During the phase angle jump tests, the charger exhibited consistent performance without any significant alterations in either the active and reactive power magnitudes. Moreover, the charger withstood all the tests without any disruptions.

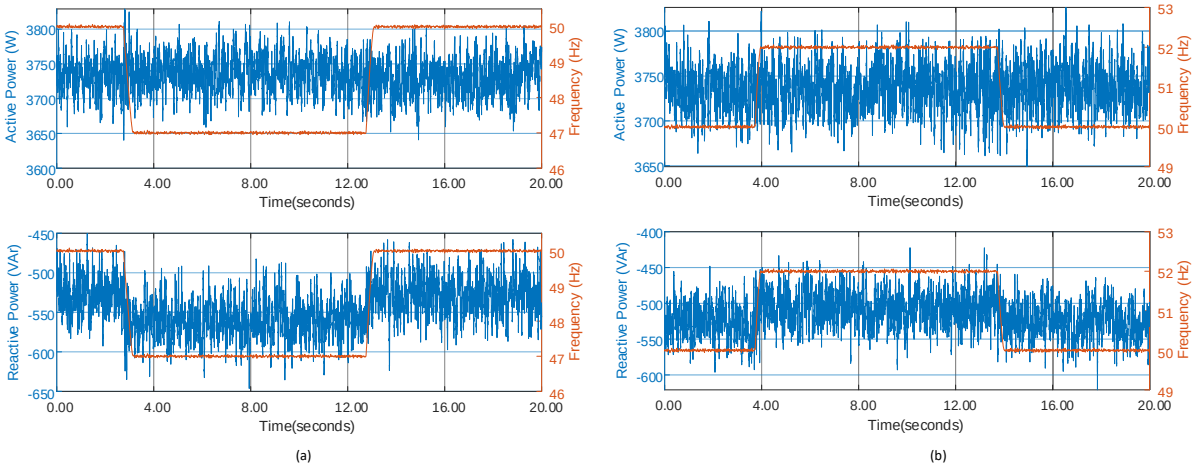


Figure 27. EV charger response to step frequency disturbances: (**a**) 50 Hz to 47 Hz, and (**b**) 50 Hz to 52 Hz.

6. Summary of Key Findings

6.1. Key Insights

6.1.1. Insights into Load Response

The experimental results provide several important insights into the response of modern residential loads to grid disturbances. Responses to voltage sags confirm the presence of capacitor current overshoots and motor inrush currents that are not represented in the present RMS composite load models. As electromagnetic transient (EMT) implementations

of composite load models are developed, these measurements can be used to incorporate such characteristics directly into EMT representations.

The applied disturbance set was selected to reflect common disturbance types and ranges observed in practice and used in composite load assessment. The purpose of the experiments is to characterise practical device behaviour under representative events and to identify response features that may not be captured in commonly used RMS composite load representations and parameter sets. The work is not intended as a comprehensive parametric sensitivity study of disturbance magnitudes and durations. Instead, the results form a foundation for subsequent modelling and broader parameter sweeps, including EMT studies where fast transients such as inrush current and capacitor charging current in SMPS-type devices can be represented explicitly.

The present RMS implementation of the composite load model also fails to incorporate phase angle jumps that are often observed after transmission system faults. The results of this study provide preliminary quantitative information that can be used to introduce phase angle jump behaviour into EMT models and to refine RMS approximations for studies of post-fault voltage recovery. For most appliances, the tests show only temporary power cessation during disturbances, with a return to normal operation once the disturbance is cleared. A notable exception is inverter-based air conditioners, which tended to disconnect under certain voltage sag events.

Appliances with inverter-based interfaces, such as refrigerators and air conditioners, generally continued normal operation for disturbances that caused their traditional direct-on-line counterparts to stall. This supports their representation as electronic loads within the composite load model, provided that appropriate disconnection thresholds and reconnection delays are included. Electronic loads were largely unaffected by frequency disturbances, except for the inverter-based microwave oven. The approximately linear relationship observed between its power consumption and frequency suggests that some electronic loads may exhibit non-negligible active and reactive power sensitivity to frequency variations, a behaviour that is not presently captured in standard CMPLDW parameter sets.

Most tested loads were not significantly affected by phase angle jump disturbances, apart from the direct-on-line motor-based refrigerator and air conditioner, for which severe phase angle jumps led to stalling and prolonged elevated currents. Static loads behaved in line with the assumptions of the composite load model, acting effectively as constant impedance, constant current, or constant power loads, depending on device type. Similar to previous DER inverter testing, repeating tests across multiple devices of the same category revealed substantial diversity in disturbance response, particularly for inverter-based air conditioners. This diversity indicates that composite load models for residential feeders should employ parameter ranges or probabilistic descriptions rather than single typical parameter sets.

These experimental results highlight why parameter tuning and classification in RMS composite load modelling need to be revisited for modern residential demand. Several electronically interfaced loads and inverter-based appliances exhibit RMS active and reactive power trajectories that differ from classical induction motor-dominated assumptions, and EV charging can introduce logic-based disconnection and reconnection behaviour that alters post-disturbance recovery. The measurements therefore provide practical evidence to support improved classification and tuning of composite load model parameters, and they also indicate when EMT-based modelling becomes important for study types where short duration transient behaviour is material.

The results in this paper are intended to support RMS composite load modelling for disturbance studies by providing experimental evidence for load classification and

parameter tuning. The tests are device-level and performed under controlled laboratory disturbances, so feeder-level studies require aggregation and weighting consistent with the feeder composition and, where possible, validation against field measurements. The work is not intended to represent EMT-scale sub-cycle transients, although the measurements help identify cases where EMT-based modelling is more appropriate. EV results are based on a limited platform, and broader testing is required to quantify variability across EVs and chargers.

Existing approaches used in disturbance and voltage recovery studies range from static voltage-dependent representations such as ZIP and exponential load models, to induction motor-based dynamic representations, and composite RMS load models that combine static and motor components, such as CMPLDW-type structures. Static models are simple and can represent steady state voltage dependence, but they cannot represent protection-driven disconnection and reconnection or the distinct trajectories observed in electronically interfaced loads and EV charging. Motor-based representations can capture stalling and recovery behaviour for motor-dominated loads, but they can misrepresent inverter-based appliances and SMPS-type devices when these are grouped into generic motor fractions. Composite RMS models provide a practical balance for system studies, but their accuracy depends strongly on correct classification and parameter tuning for modern residential demand.

In this context, the contribution of this paper is experimental. The measured RMS active and reactive power trajectories provide evidence for where common assumptions used in existing RMS composite models can be insufficient for modern residential loads, and they support improved classification and tuning within an established composite modelling framework. The experiments also identify behaviours, such as inrush and capacitor charging effects in SMPS-type devices, that motivate EMT-based modelling for study types where short duration or sub-cycle behaviour is material.

6.1.2. Insights into EV Charger Response

The present composite load model does not include a dedicated component to represent EVs or EV chargers. The experimental results indicate that residential EV chargers exhibit behaviours that are distinct from both traditional motor loads and generic electronic loads. Many small residential EV chargers comprise electrical relays, communication and control elements, and protection functions, while relying on the on-board power electronics of the vehicle for power conversion. Consequently, the response of the combined charger and EV to a grid disturbance depends on both the internal logic of the charger and the control strategy of the vehicle.

The tests indicate that Level 1 chargers can be approximately characterised as constant current devices across a broad range of voltage sags, with disconnection and delayed reconnection when the voltage falls below device-specific thresholds. In contrast, the tested Level 2 charger behaved more like a constant power device during swell events and rode through all sag tests, with only transient changes in active and reactive power. These behaviours are not adequately captured by the existing CMPLDW structure and motivate the introduction of an explicit EV charger block with separate parameterisation for Level 1 and Level 2 devices and for different charger and vehicle combinations.

Given that EV charging behaviour depends on the composition of the EV fleet, a stochastic modelling approach for residential EV chargers is likely to be more appropriate than a deterministic one. Since only one EV was available during this stage of the project, further testing involving a wider range of EVs and charger technologies is required to generalise the proposed modelling approach. Fast chargers (or Level 3 chargers), which incorporate active power electronics, can mitigate the impact of individual EVs on grid

disturbances and may have very different disturbance responses. Such devices were not included in the present tests and will be the subject of future work.

6.2. Recommendations and Reclassification

Based on the experimental results, several recommendations can be made for the use and refinement of composite load models in distribution level studies. First, inverter-based refrigerators and split-system air conditioners should be represented as electronic loads within the CMPLDW framework, while conventional direct-on-line motor devices are retained in the Motor D category. Parameter sets for the electronic load block should include voltage sag-induced disconnection thresholds and reconnection delays consistent with the observed behaviour. Second, LED lighting should be modelled as an electronic load with clearly defined sag thresholds that lead to a momentary cessation of power, reflecting the observed flicker and complete power loss when the voltage is reduced below a certain level.

Third, vacuum cleaners, pedestal fans, and similar small direct-on-line motor appliances can continue to be represented within Motor D; however, parameterisation should be refined to capture transient inrush currents and stalled operation for deep sags and severe phase angle jumps. Finally, a dedicated EV charger component should be introduced into the composite load model structure. This component should include distinct modes for Level 1 and Level 2 chargers, for example, constant current versus constant power response, and should capture sag ride-through, disconnection behaviour, and reconnection dynamics informed by the laboratory measurements. These steps are expected to reduce the mismatch between the modelled and observed behaviour of modern residential loads and to improve the robustness of stability studies performed by NSPs and system operators.

The laboratory disturbances applied in this study are intentionally controlled and repeatable so that device-level behaviour can be isolated and compared across load types. Aggregate feeder behaviour can differ due to the diversity of devices, coincidence, background operating conditions, and interactions with network impedance and controls. For this reason, the results are intended to inform load classification and parameter tuning within composite load modelling, rather than directly represent any particular feeder without calibration. Feeder-level application requires appropriate aggregation and weighting of device classes and, where possible, validation against field measurements.

7. Conclusions and Future Work

This paper details an extensive laboratory study of the response of modern residential loads and EV chargers to voltage magnitude, frequency, and phase angle disturbances representative of events in practical distribution networks. The results confirm that many appliances exhibit dynamic behaviour such as capacitor inrush currents, stalled motor operation, and voltage dependent disconnections that are not captured in the presently deployed RMS composite load models used in the NEM. The measurements provide a coherent data set that can be used to adjust parameter ranges for Motor D and electronic load components and to guide the development of new model elements for EV chargers.

For NSPs and system operators, the findings highlight that the aggregate residential load seen at higher voltage levels is increasingly dominated by inverter-based devices whose disturbance response is governed by embedded control and protection logic. Continued reliance on legacy ZIP models or poorly tuned composite load models may therefore lead to inaccurate predictions of voltage recovery, fault-induced delayed voltage recovery, and system stability margins. Incorporating empirically validated models for key residential device classes is an important step towards more reliable planning and operational studies in power systems with high DER penetration.

https://doi.org/10.3390/en19020493

Future work will focus on several directions. Additional testing of other motor types, including water pumps and commercial refrigeration systems, will be undertaken to complete the coverage of CMPLDW components. A broader set of EVs and charger technologies, including fast chargers, will be tested to develop and validate a generic EV charger model suitable for both RMS and EMT simulations. The detailed development and validation of a dedicated EV model block for the CMPLDW also needs to be considered. Finally, the laboratory-derived parameter sets will be applied in case studies on representative NEM feeders, combining field measurements (i.e., including non-ideal disturbances) and dynamic simulations to quantify the impact of revised load models on system-wide stability assessments.

Author Contributions: Methodology, O.R., S.E., D.A.R. and J.R.; Validation, O.R., S.E., D.A.R. and J.R.; Investigation, O.R., S.E., D.A.R. and J.R.; Software, O.R., S.E., D.A.R. and J.R.; Resources, S.E. and D.A.R.; Writing—original draft, O.R.; Writing—review & editing, S.E., D.A.R. and J.R.; Supervision, S.E., D.A.R. and J.R. All authors have read and agreed to the published version of the manuscript.

Funding: This research was funded by the CSIRO under the Australian Research Program for System Transformation (ARPST), Topic 9 "Distributed Energy Resources and Stability", Stage 4, Grant Number RG241337.

Data Availability Statement: The data presented in this study are openly available in [Data] at [http://pvinverters.ee.unsw.edu.au/] (accessed on 5 July 2023) [19].

Acknowledgments: The authors gratefully acknowledge the DER Operations team at the Australian Energy Market Operator (AEMO) for their collaboration, provision of disturbance data, and feedback on the experimental program. This work was supported by CSIRO under the Australian Research Program for System Transformation (ARPST), formerly the Global Power System Transformation (G-PST) program, Topic 9 "Distributed Energy Resources and Stability". The authors also thank the broader ARPST Topic 9 project team and steering committee for their constructive discussions, which informed the experimental design and interpretation of results.

Conflicts of Interest: Author Jenny Riesz was employed by the company Australian Energy Market Operator. The remaining authors declare that the research was conducted in the absence of any commercial or financial relationships that could be construed as a potential conflict of interest.

Abbreviations

The following abbreviations are used in this manuscript:

AEMO	Australian Energy Market Operator
ARPST	Australian Research Program for System Transformation
BESS	Battery energy storage system
CMPLDW	WECC composite load model
CSIRO	Commonwealth Scientific and Industrial Research Organisation
DER	Distributed energy resource
DOL	Direct-on-line
EMT	Electromagnetic transient
EV	Electric vehicle
G-PST	Global Power System Transition
LED	Light emitting diode
NEM	National Electricity Market
NERC	North American Reliability Corporation
NSP	Network Service Provider
PV	Photovoltaic
RoCoF	Rate of change of frequency
RMS	Root Mean Squared
SoC	State of Charge

VFD	Variable frequency drive
WECC	Western Electricity Coordinating Council
ZIP	Impedance Current Power Static Load Model

References

1. Cutsen, T.V.; Vournas, C. *Voltage Stability of Electric Power Systems*; Kluwer: Norwell, MA, USA, 1998.
2. Mauricio, W.; Semlyen, A. Effect of Load characteristic on the Dynamic Stability of Power Systems. *IEEE Trans. Power Appar. Syst.* **1972**, *PAS-91*, 2295–2304. [CrossRef]
3. Pourbeik, P.; Ryan, D.; Brnadic, F.; Riesz, J.; Badrzadeh, B.; Lu, J. Developing Dynamic Load Models for the Australian National Electricity Market with a Focus on Distributed Energy Resources. *CIGRE Sci. Eng.* **2021**, *20*, 91–105.
4. Terzija, V.; Valverde, G.; Cai, D.; Regulski, P.; Madani, V.; Fitch, J.; Skok, S.; Begovic, M.M.; Phadke, A. Wide-Area Monitoring, Protection, and Control of Future Electric Power Networks. *Proc. IEEE* **2011**, *99*, 80–93. [CrossRef]
5. Wen, J.Y.; Jiang, L.; Wu, Q.H.; Cheng, S.J. Power system load modeling by learning based on system measurements. *IEEE Trans. Power Deliv.* **2003**, *18*, 364–371. [CrossRef]
6. Rahman, O.; Muttaqi, K.M.; Sutanto, D. Time Series Variations of the Neutral-to-Ground Potential in a 4-Wire LV Network under Unbalanced Allocation of Rooftop Solar PV and Mitigation using Energy Storage. In Proceedings of the 2019 IEEE Power & Energy Society General Meeting (PESGM), Atlanta, GA, USA, 4–8 August 2019; pp. 1–5. [CrossRef]
7. Austalian Energy Market Operator (AEMO). *PSSE Models for Load and Distributed PV in the NEM: Model Development and Validation*; The Australian Energy Market Operator: Melbourne, VIC, Australia. Available online: https://www.aemo.com.au/-/media/files/initiatives/der/2022/psse-models-for-load-and-distributed-pv-in-the-nem.pdf (accessed on 5 July 2023).
8. Arif, A.; Wang, Z.; Wang, J.; Mather, B.; Bashualdo, H.; Zhao, D. Load Modeling—A Review. *IEEE Trans. Smart Grid* **2018**, *9*, 5986–5999. [CrossRef]
9. Australian Energy Market Operator (AEMO). *Validation of Dynamic Models for Distributed PV and Composite Load: Benchmarking of DERAEMO1 and CMLD Models in PSSE Against Disturbances*; The Australian Energy Market Operator: Melbourne, VIC, Australia, 2025. Available online: https://www.aemo.com.au/-/media/files/initiatives/der/2025/validation-of-dynamic-models-for-distributed-pv-and-composite-load_2025.pdf (accessed on 5 October 2025).
10. Jayasinghe, H.; Gunawardane, K.; Nicholson, R. Applications of Electrical Load Modelling in Digital Twins of Power Systems. *Energies* **2025**, *18*, 775. [CrossRef]
11. Kosterev, D.; Meklin, A.; Undrill, J.; Lesieutre, B.; Price, W.; Chassin, D.; Bravo, R.; Yang, S. Load modeling in power system studies: WECC progress update. In Proceedings of the 2008 IEEE Power and Energy Society General Meeting—Conversion and Delivery of Electrical Energy in the 21st Century, Pittsburgh, PA, USA, 20–24 July 2008; pp. 1–8. [CrossRef]
12. Shaffer, J.W. Air conditioner response to transmission faults. *IEEE Trans. Power Syst.* **1997**, *12*, 614–621. [CrossRef]
13. Williams, B.R.; Schmus, W.R.; Dawson, D.C. Transmission voltage recovery delayed by stalled air conditioner compressors. *IEEE Trans. Power Syst.* **1992**, *7*, 1173–1181. [CrossRef]
14. North Americal Electric Reliability Coorporation. Draft Dynamic Load Modeling: Technical Reference Document—Dynamic Load Modeling. August 2025. Available online: https://www.nerc.com/globalassets/who-we-are/standing-committees/rstc/0-rstc-agenda-links/20251210_1_14_draft_dynamic-load-modeling-technical-reference_2025_8_19_lmwg_approved-redline.pdf (accessed on 15 January 2026).
15. Haidar, A.M.A.; Muttaqi, K.M. Behavioral Characterization of Electric Vehicle Charging Loads in a Distribution Power Grid Through Modeling of Battery Chargers. *IEEE Trans. Ind. Appl.* **2016**, *52*, 483–492. [CrossRef]
16. Phan, Q.B.; Rahman, O.; Elphick, S. Empirical EV Load Model for Distribution Network Analysis. *Energies* **2025**, *18*, 3494. [CrossRef]
17. Konstantinou, G.; Ahmad, A.; Rahman, O.; Elphick, S.; Robinson, D.; Fletcher, J.; Riesz, J.; Graham, P. *GPST Topic 9: DER and Stability—Stage 2 Final Report*; University of Wollongong: Wollongong, NSW, Australia, 2025. Available online: https://ro.uow.edu.au/articles/report/GPST_Topic_9_DER_and_Stability-_Stage_2_Final_Report/30496907 (accessed on 19 November 2025).
18. Rahman, O. Composite Load Model Motor D Testing. In *Report for CSIRO, Australian Power Quality Research Centre*; University of Wollongong: Wollongong, NSW, Australia, 2024.
19. Ahmadyar, S.; Callegaro, L.; Monrroy, C.R.; Konstantinou, G.; Riesz, J.; Fletcher, J. *Inverter and Load Testing Results*; University of New South Wales: Sydney, NSW, Australia. Available online: http://pvinverters.ee.unsw.edu.au/ (accessed on 5 July 2023).

Disclaimer/Publisher's Note: The statements, opinions and data contained in all publications are solely those of the individual author(s) and contributor(s) and not of MDPI and/or the editor(s). MDPI and/or the editor(s) disclaim responsibility for any injury to people or property resulting from any ideas, methods, instructions or products referred to in the content.